Perspective

On the Surface Compositions of Molybdenum Carbide Nanoparticles for Electrocatalytic Applications

Siying Yu and Hong Yang *

Department of Chemical and Biomolecular Engineering, University of Illinois Urbana-Champaign, 600 S. Mathews, Urbana, IL 61801, USA

* Correspondence: hy66@illinois.edu

Received: 28 November 2024; Accepted: 2 December 2024; Published: 6 December 2024

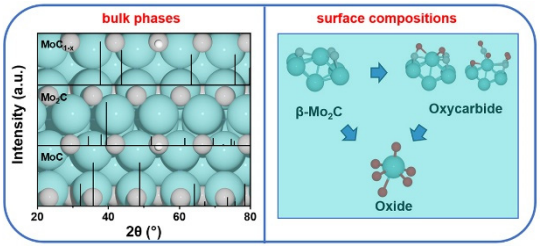

Abstract: Molybdenum carbide has attracted much research attention for its precious metal-like catalytic properties, especially in hydrogen-involved reactions. It possesses rich crystal and surface structures leading to different activity and product selectivity. With advances in nanoengineering and new understanding of their surfaces and interfaces, one can control the transition between different phases and surface structures for molybdenum carbide nanoparticles. In this context, it is essential to understand their surface compositions and structures under operating conditions in addition to their intrinsic ones under ambient conditions without external cues. The necessity of surface study also comes from the mild oxidation brought by passivation in carbide nanoparticles. made using the bottom-up synthesis or solid-gas phase temperature-programmed reduction. In this perspective, we first introduce the relevant crystal structures of molybdenum carbides and highlight the features of the three types of chemical bonding within. We then briefly review the studies of thermodynamically favored surface components and nanostructures for partially oxidized molybdenum carbide nanoparticles based on both experimental and theoretical data. An electrochemical oxidation method is used to illustrate the feasibility in controlling and understanding the surface oxidation. Finally, structure-property relationship is discussed with several recent examples, focusing on the effect of phase dependency on the adsorption energy of reaction intermediates.

Keywords: molybdenum carbide; surface composition; oxycarbide; electrocatalysis; hydrogen evolution reaction; density functional theory

1. Introduction

Renewable energy such as hydropower, wind, solar, and biofuel occupies a growing share of global energy consumption, playing an important role in steadily reducing the dominant status of fossil fuels. Sustainable electrochemical technologies focusing on fuel cells, electrolyzers for water splitting, and batteries have been intensively studied for their large-scale commercialization [1,2]. Design of electrocatalysts and electrode materials is crucial to bring out the maximum activity and durability of the energy devices, achieving both energy- and cost-efficiency. Noble metals such as platinum and palladium are conventional electrocatalysts but less favorable due to their high cost [3,4]. As potential substitutions for precious metals, molybdenum carbide (Mo_xC) materials have been widely studied for their application in electrochemical catalysis, especially for hydrogen evolution reaction (HER) [5,6] oxygen evolution reaction (OER) [7], nitrogen reduction reaction (NRR) [8], and carbon dioxide reduction reaction (CO_2RR) [9]. While the mechanisms for their Pt-like properties are still under investigation, it has been reported that the (111) surface of β-Mo_2C exhibits comparable Gibbs free energy to that of Pt (111) plane [10]. After modification of surface components of carbide materials, a balanced adsorption/desorption of reacting species, intermediates, and products on catalyst surface can be achieved, which is beneficial to facilitate the kinetics of a target reaction [11,12]. Considerable approaches have been examined, such as exposing active sites by nanoengineering [13,14], surface modification using heteroatom doping [12,15], interface engineering by incorporation of catalyst supports [16,17], and structural design using porous and hierarchical materials [18,19].

All strategies require a comprehensive understanding of surface compositions of Mo_xC and how these compositions may modify the interaction between surface sites and reactants.

The necessity to understand surface components also arises from the synthetic conditions of Mo_xC materials. Using β-Mo_2C as an example, it can be made in three major approaches: solid-solid, solid-liquid, and solid-gas methods [20,21]. In a solid-solid phase method, carbon is used as support in the process of carburization of Mo precursors. The synthesis is carried out at high temperatures (>1500 °C) to overcome the energy barrier of carbon diffusion into Mo lattice, resulting in large particle size, low specific surface area, and inferior catalytic properties [18,22]. The solid-liquid phase method, which usually uses urea glass, alcohol, and phenolic resin as the carbon source, can reduce the reaction temperature to 600~900 °C [20,21].

An effective, current synthesis is based on solid-gas phase temperature programmed reduction (TPR) method. In this approach, hydrocarbon gases such as methane may be reduced by hydrogen gas to produce the carbon in metal carbides, which greatly lowers the synthetic temperature to make nanometer (nm)-sized carbide particles [23,24]. The benefit of using gaseous carbon sources includes flexibility in the choice of catalyst support, especially allowing for a delicate size and morphology control of carbide nanoparticles. The choice of carbon-containing gas is also reported to affect the structure of the obtained carbide [20,25]. Using solid-gas synthesis may have its challenges as well. The incomplete combustion of excess carbon-containing gases may result in the formation of carbon residue on carbide surface [26]. The carbon residue not only complicates the microscopic study of carbide nanomaterials but also deactivates the surface. As Mo_xC nanoparticles are pyrophoric due to their highly reactive surfaces, post-treatment, such as mild passivation, may also be needed for their safe use under ambient conditions [27], resulting in surface oxidation [23]. The partially oxidized surface, known as oxycarbide, can be either carbidic or oxidic based on oxygen coverage [28]. There is much research interest in characterizing the surface of oxidized molybdenum carbide [29,30] and studying the impact of controlled oxidation on catalytic properties [23,31,32], because surface composition often determines catalytic activity.

In this Perspective, we highlight the understanding of surface compositions of Mo_xC nanoparticles and their effects on electrochemical catalysis. We first present the crystal structures and summarize the key relevant features of chemical bonding in Mo_xC. We then discuss the thermodynamically favored surface components and nanostructures of partially oxidized Mo_xC nanoparticles based on both experimental and theoretical data. Relationship between catalytic properties and compositional and structural parameters of Mo_xC nanocatalysts is explained based on adsorption energy of reaction intermediates. The effects of phase dependency on catalytic applications are highlighted using selected recent examples.

2. Structure of Molybdenum Carbides and Key Features of Chemical Bonding

Molybdenum carbides can be regarded as interstitial compounds, where large transition Mo atoms serve as the host lattice, and small carbon atoms occupy the interstitial vacancies. Experimentally, X-ray diffraction (XRD) is a common technique to study the crystal structure of Mo_xC. There are mainly three types of packing structures for interstitial carbides, i.e., face-centered cubic (*fcc*), hexagonal closed packed (*hcp*), and simple hexagonal (*hex*) structures. Their corresponding standard XRD patterns are illustrated in Figure 1. In a cubic structure, each Mo atom is surrounded by six C atoms. The hexagonal Mo_xC forms a structure with alternating Mo and C layers [33].

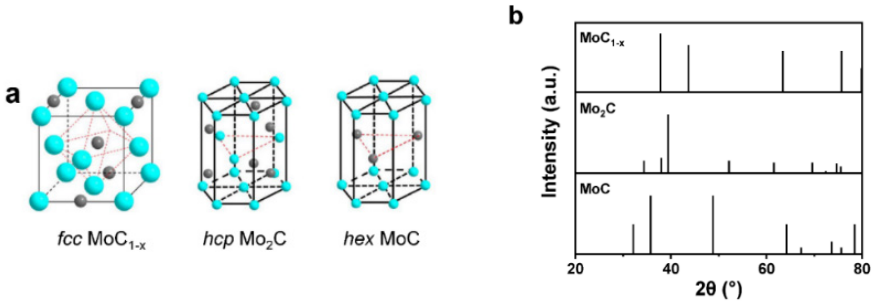

Figure 1. (**a**) Illustration of the three common Mo_xC crystal structures. Reprinted with permission from Ref. [34]. (**b**) The corresponding standard XRD patterns of MoC_{1-x}, Mo_2C, and MoC.

There are three kinds of bonding in the Mo_xC materials, i.e., metallic bond between Mo atoms, covalent bond between Mo and C, and ionic bond caused by charge transfer between Mo and C. The electron localization function (ELF) topological analysis was applied to study the chemical bonding in molybdenum carbide nanoparticles [35].

A detailed electronic structure calculation shows the local maxima of electron density are contained in a basin as illustrated in the isosurfaces of each configuration (Figure 2a–c). The core basin (i.e., C(X), X = Mo or C) contains a nucleus meanwhile the valence basin (i.e., V(*m*X, *n*Y), X, Y = Mo or C, *m* and *n* are integers) includes a number of core basins. For Mo_1C_1 configuration, the electron density maximum is found 0.624 Å from Mo and 1.067 Å from C, with a low basin population of 0.2e. This calculation implies the ionic character of the Mo-C bonding (Figure 2a). In contrast, two bonding basins of Mo-C (i.e., V(C, Mo)) in the Mo_2C_1 configuration have 1.8e, indicating a significant change to a more covalent character (Figure 2b). The ELF method was further applied to a more complex $Mo_{28}C_{14}$ configuration regarding its Mo-terminated surface. Three-center basins V(3Mo) and four-center basins V(C, 3Mo) are observed and reported to related to the three kinds of three-fold hollow sites (V_C, H_M, H_C) for surface adsorption [36].

Analysis of density of states (DOS) is another method to investigate the electronic structure of Mo_xC [33]. Different phases of Mo_xC have different C 2s bands in shape and energy between −10.5 and −13.5 eV (Figure 2d). For δ-MoC and α-MoC, the bands around the Fermi energy (E_F) have a narrow close-to-zero region, which separates the whole band into the covalent bonding and antibonding areas (Figure 2d,e). These two regions are composed of C 2p and Mo 5d electrons, though the metallic nature of carbide mainly comes from Mo. The DOS of δ-MoC has the sharpest peaks, indicating the most localized distribution of electrons and mixed ionic-covalent bonding. For β-Mo_2C, however, it has the most metallic character because E_F is within the electronic bands. Due to the strong interaction between carbon and metal atoms, Mo_xC (e.g., Mo_2C) possesses a high melting point (2520 °C) with its electric and thermal conductivity similar to ceramics [34]. These properties make them attractive functional materials, especially after they were found to exhibit catalytic activity in electrochemical reactions [5,37,38].

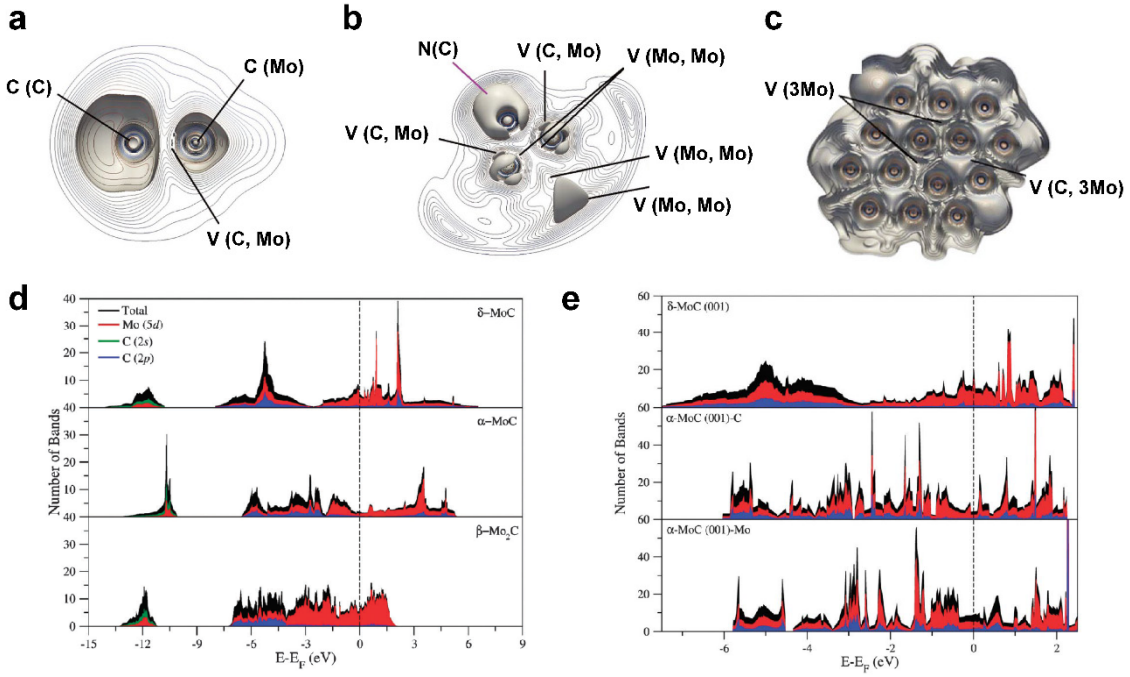

Figure 2. ELF isosurfaces of (**a**) Mo_1C_1, (**b**) Mo_2C_1, and (**c**) $Mo_{28}C_{14}$ complexes. V(X, Y) indicates the valence basin between two centers (X, Y = C or Mo), and C(C) and C(Mo) indicate a carbon and molybdenum core basin, respectively. Reprinted with permission from Ref. [35]. (**d**) Total and projected DOS for Mo_xC with different bulk structures. (**e**) Projected DOS for the most stable low Miller-index surfaces of δ-MoC and α-MoC phases. Reprinted with permission from Ref. [33].

3. Surface Composition: Experimental and Quantum Simulation Studies

3.1. Phase Behaviors of Mo_xC Nanomaterials

Size and composition control is crucial in synthesizing Mo_xC nanomaterials to bring out their precious metal-like catalytic properties. Molybdenum carbides have been reported to exhibit multiple crystal structures (Figure 3a) and reactions conditions can be modified to prepare different targeted products. The transition between different carbide structures becomes easier when the particle size is reduced to nm-sized scale. The large surface

area-to-volume ratio means contribution of surface energy to the total energy becomes significant, making those metastable phases with low surface energy becomes thermodynamically preferable at small sizes (Figure 3b–d) [14]. In another word, nanosized carbide particles may have different phases from those suggested by the conventional phase diagram (Figure 3b). To obtain this size-dependent phase diagram, the bulk free energy values ($\Delta\Omega_{bulk}$) of different Mo_xC were estimated as a function of the chemical potential of carbon ($\Delta\mu_C$) (Figure 3c). Surface energies were incorporated into the calculation of size-dependent free energy based on the Gibbs-Thomson equation. It is also necessary to optimize the computed Wulff constructions based on equilibrium particle morphologies of different carbide phases to address the relationship between surface energy and Miller index (Figure 3d). Combining both bulk phase and surface energy terms, δ-MoC phase dominates in the size regime of <3.3 nm and α-Mo_2C phase is the preferable product in the range of 3.3~40 nm. When the resulting nanoparticle is larger than 40 nm, γ-MoC and β-Mo_2C are expected to form (Figure 3b).

Other than thermodynamic considerations, the structural transformation can also be realized through formation of energetically favored interface [39]. Density functional theory (DFT) calculations suggest the feasibility of Zn-facilitated phase transformation. The adhesion energy of MoC(101)||Mo_2C(101) interface is found to be smaller than the sum of surface energy of MoC(101) and Mo_2C(101). Thus, the epitaxial growth of MoC from Mo_2C should be thermodynamically favored. A Zn-modified MoC(101)/Mo_2C(101) interface is calculated to be more stable than a Zn-free interface, further benefiting the formation of MoC/Mo_2C interface. This structural transformation can be demonstrated by the XRD patterns of carbide samples with different Zn/Mo ratios (Figure 3e). The characteristic peaks of MoC (101) and Mo_2C (101) are located at 36.3° and 39.6°, respectively. With a higher Zn/Mo feeding ratio, the peak intensity ratio between MoC (101) and Mo_2C (101) also increases. With bulky phase information characterized by XRD, researchers rely on X-ray photoelectron spectroscopy (XPS) to study the surface chemical constituents. Figure 3f shows the Mo 3d spectrum for Zn-MoC/Mo_2C-0.5. Peak deconvolution was performed to assign each XPS peak to the four oxidation states of Mo, i.e., Mo(II), Mo(III), Mo(IV), and Mo(VI). Peaks around 228.6 eV and 231.8 eV refer to Mo(II) $3d_{3/2}$ and $3d_{5/2}$ of Mo_2C, which have comparable peak intensity to those for Mo(III) of MoC. The co-existence of MoC and Mo_2C in the surface region is consistent with the XRD results as shown in Figure 3e. It should be noted that Mo(IV) and Mo(VI) are commonly observed in Mo carbide nanosized samples unless they are prepared and characterized in situ without exposure to air. These oxides are a result of surface oxidation of Mo_xC nanoparticles under ambient conditions.

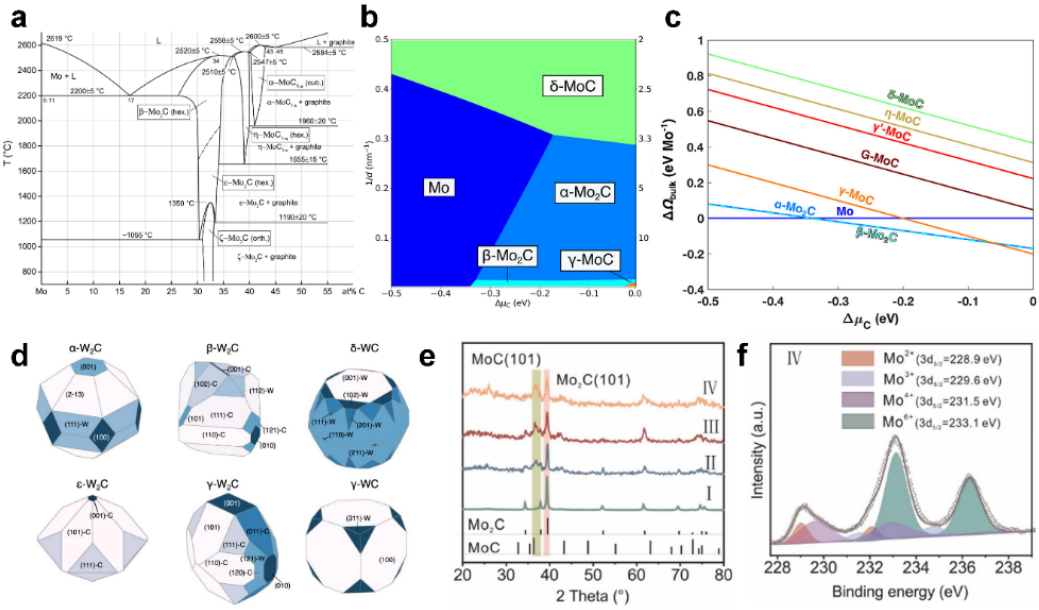

Figure 3. (**a**) Binary phase diagram of Mo and C. Reprinted with permission from Ref. [22]. (**b**) Lowest energy 2-D phase diagram by projecting 3-D diagram onto $\Delta\mu_C$-1/d axis. (**c**) Free energy of Mo_xC at different chemical potentials of carbon ($\Delta\mu_C$). (**d**) Computed Wulff constructions of the equilibrium particle morphologies of different carbide phases at $\Delta\mu_C$ = −0.15 eV. This value of $\Delta\mu_C$ was chosen because it roughly corresponds to common composition and temperature synthesis conditions. Reprinted with permission from Ref. [14]. (**e**) XRD patterns of the Zn-MoC/Mo_2C catalysts with different Zn/Mo feeding ratio (I: 0, II: 0.1, III:0.2, IV: 0.5). (**f**) High resolution XPS spectrum of Mo 3d for the Zn-MoC/Mo_2C-0.5 catalyst. Reprinted with permission from Ref. [39]. Copyright 2021 American Chemical Society.

3.2. Controlled Surface Oxidation by an Electrochemical Approach

While there is a great incentive to control the surface chemistry of metal carbide to optimize their catalytic properties, it is non-trivial to develop a proper synthetic approach with the precision that is needed. Surface oxidation can be best controlled with those Mo_xC nanomaterials made using the solid-gas synthesis [23]. This method significantly reduces the reaction temperature of Mo_xC nanomaterials, preventing severe overgrowth of carbide while enabling the exposure of active surfaces using the bottom-up synthesis. In a typical synthesis, a mixed forming gas consisting of a short-chain hydrocarbon (e.g., methane) and hydrogen is often used. Heat treatment of metal precursors in such a reducing atmosphere gives rise to the formation of highly reactive carbide nanoparticles, whose surface can be partially oxidized to result in metallic-like H-adsorption sites and Brønsted acid hydroxyl sites [40]. Catalytic properties of Mo_xC nanoparticles thus are readily tunable by the surface oxidation [41]. Controlled treatment through oxidation of surface sites was reported to help adjust the acidic site density of 2~5 nm Mo_2C nanoparticles [42]. Product selectivity could also be affected by the oxygen coverage on carbide surface [30,43].

While the solid-gas phase synthesized Mo_xC can be oxidized readily, the approach is lacking the control in the degree of oxidation. Electrochemical oxidation appears to be an ideally suited approach to making partially and fully oxidized Mo_xC nanoparticles, meeting the technical challenge on quantitatively control over the degree of oxidation. In our recent study, different degrees of surface oxidation were achieved by applying predetermined upper limit of oxidation potential in an aqueous electrolyte, shown in cyclic voltammetry (CV) (Figure 4a) [23]. In this synthesis, electrooxidation of β-Mo_2C could occur at an onset potential of around 0.6 V (vs. RHE) and the peak current density was achieved at ~0.8 V. When the upper limit was raised to 1.2 V, the oxidation current density was close to zero, suggesting a complete surface oxidation. X-ray photoelectron spectroscopy (XPS) study indicates the complete surface oxidation started at a high potential, ranging from 0.975 V and 1.2 V. Our XPS study indicates the carbidic peaks appearing between 0.4 V and 0.85 V in Mo spectra can be assigned to (Mo) oxycarbides.

Our density functional theory (DFT) simulations further catch this change from carbides, to oxycarbides, and ultimately to oxides in detail, providing strong atomic analysis of relationship between surface structure and degree of oxidation (Figure 4c–f). Oxygen-covered surface configurations are thermodynamically more stable than those of oxygen-free configurations across the potential range from 0 to 0.6 V (Figure 4d). In the range of 0 to 0.28 V, 1/3 of Mo sites and all C sites are covered with oxygen ($(Mo\text{-}O)_1(C\text{-}O)_6$). The DFT simulation also reveals that, on a carbon-terminated facet, surface carbon is more sensitive to oxidation than surface Mo, which is consistent with our spectroscopic data. When the oxidation potential increases, the surface oxycarbide structure transforms into more oxidized configurations, i.e., $(Mo\text{-}O)_3(C\text{-}O)_6$) and $(Mo\text{-}O)_4(C\text{-}O)_6$. Our quantum simulation results further indicate a fully oxygen-covered carbide surface may be on a nanoparticle that is not fully oxidized. With an oxidation potential higher than 0.6 V, a substitutional oxidation pathway may occur, where oxygen-covered surface carbons further react to form CO and CO_2 species. These carbon derivatives subsequently desorb from the surface, exposing carbide subsurfaces, allowing oxidization of sublayer Mo and C sites, and triggering the structural transformation from oxycarbide to oxide (Figure 4e). The DFT simulation suggests such a process is thermodynamically favorable at a wide range up to an oxidative potential of 1.2 V and explains the experimentally observed peak current density around 0.8 V in CV scans (Figure 4a).

The DFT and experimental studies developed for β-Mo_2C nanoparticles were applicable to analyze the surface composition of α-MoC [44]. Both computational and experimental data indicate that α-MoC is more resistant to electrochemical oxidation than β-Mo_2C, i.e., the surface structural transformation of α-MoC to oxycarbide and oxide is more difficult (Figure 5a–c). This resistance to oxidation is attributed to the unfavored substitutional oxidation. The ab initio thermodynamics calculation suggests α-MoC(311)-Mo and β-Mo_2C(011)-C surfaces as the most dominant facets under synthetic conditions. Considering the adsorption of O*/OH*/H*, the pH-dependent surface Pourbaix diagram for α-MoC(311)-Mo facet was obtained (Figure 5a). At pH = 1, the oxidized surface, with all Mo_{fcc} sites and half of C_{top} sites covered with oxygen, is stable up to 0.71 V. A structural transformation from $(Mo\text{-}O)_8(C\text{-}O)_4$ to $(Mo\text{-}O)_8(C\text{-}O)_5$ configuration happens in the potential range from 0.71 to 0.84 V. This conversion is limited by H_2O dissociation and is thus considered as a slow oxidation. After reaching 0.84 V, the product, $(Mo\text{-}O)_8(C\text{-}O)_5$, becomes thermodynamically favorable, thus promoting the reaction rate of surface oxidation. Further oxidation is expected if the oxidative potential is above 0.84 V at pH = 1. For β-Mo_2C, however, the slow and fast oxidation steps happen at the potential of 0.23 and 0.46 V, respectively (at pH = 1 in Figure 5b). This stability analysis is based on the thermodynamically stable (311)-Mo facet of α-MoC. It appears the metal-terminated surface adds to the difficulty of oxidation and retards the oxidation of C atoms to CO and CO_2 species. In contrast, the carbon-terminated β-Mo_2C(011)-C facet may react with O* and form mobile CO*

species. The experimental results show a more pronounced and broader oxidation peak for β-Mo_2C than α-MoC (Figure 5c), which is consistent with the theoretical predictions.

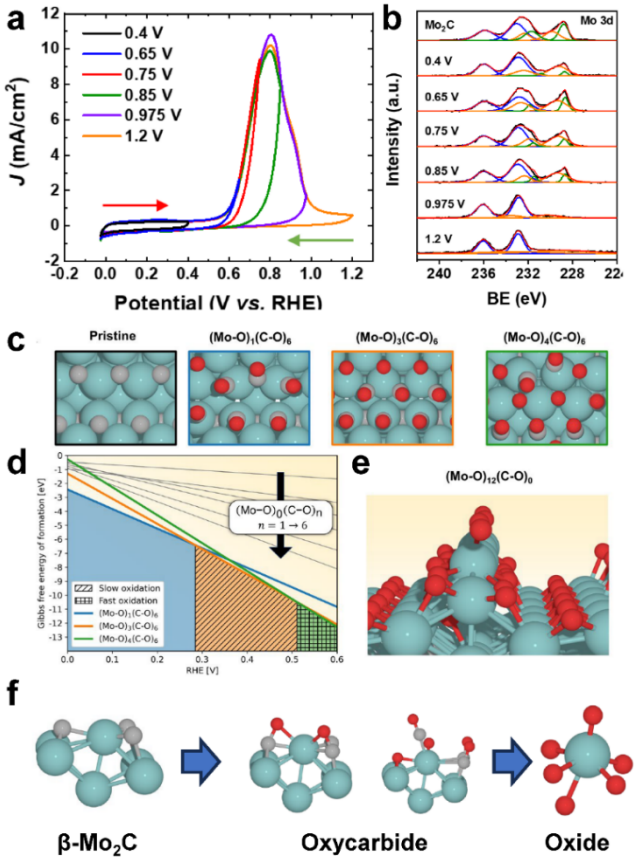

Figure 4. (**a**) CV curves for the electrochemical surface oxidation (red arrow: direction of the forward scan; green arrow: direction of the back scan). (**b**) XPS of Mo 3d regions (blue: VI; orange: IV; green: II), showing the evolution of surface compositions as a function of the upper limit of potential used in the electrochemical oxidation process. The black lines are obtained XPS curves, and the red lines are fitting envelopes. (**c**) Models of top view of thermodynamically stable β-Mo_2C(011) carbon-terminated surfaces. The pristine surface is included for reference. (**d**) Gibbs free energy of formation as a function of applied potential computed by the DFT simulation. (**e**) Proposed surface oxide structure formed after the complete oxidation in hatched regions at a high potential (cyan: Mo; grey: C; red: O). (**f**) Illustrations of nearest neighboring atoms for a given Mo at different surface coverages. Reprinted with permission from Ref. [23].

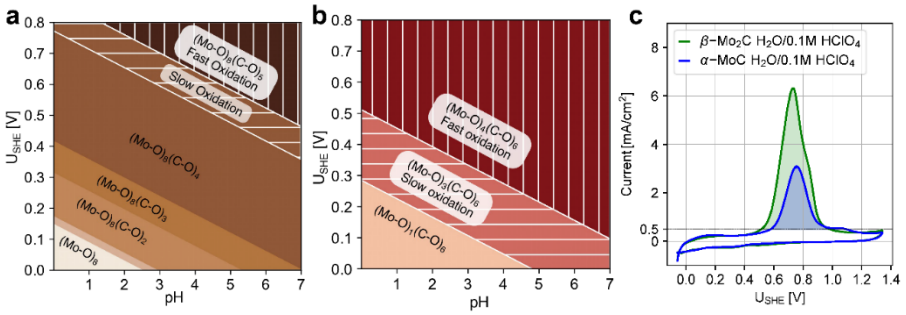

Figure 5. (**a**) Surface Pourbaix diagram for α-MoC considering the adsorption of O*/OH*/H*. Horizontal hatches show slow oxidation, and the vertical hatch corresponds to facile fast oxidation through CO desorption. At pH = 1, the onset potentials for each region starting with $(Mo\text{-}O)_8(C\text{-}O)_1$ are 0.09, 0.11, 0.25, 0.34, and 0.84 V, respectively. (**b**) Surface Pourbaix diagram for β-Mo_2C(011) considering only O* coverage. (**c**) CV for α-MoC and β-Mo_2C in an aqueous solution (pH = 1). The shaded area corresponds to the region of the CV curve considered for the charge transfer calculation. The threshold current used is 0.5 mA/cm_2. Reprinted with permission from Ref. [44].

4. Electrocatalysis of Molybdenum Carbide Nanoparticles

Properties of electrocatalysts are closely related to the adsorption/desorption of reactants, their intermediates and final products. Catalytic performance of Mo_xC is often dependent on different structural factors, including crystal phase, metal dopant, and Mo valence. Dependency of performance on surface structures can be illustrated through hydrogen evolution reaction (HER) by Mo_xC electrocatalysts. Figure 6 shows the results of a theoretical study of the effects of twenty-nine atomic configurations of seven different surfaces on HER [11], including their atomic configuration, stability, and adsorption of O* and HO*. Figure 6a shows the free-energy change of hydrogen (ΔG_H) at different hydrogen coverages on the bare, oxygenated, hydroxylated, or oxygenated/hydroxylated surfaces. The exchange current densities for each surface were derived to reflect their predicted HER activities (Figure 6b). An absolute value of 0.20 eV of ΔG_H is regarded as too large for a favorable adsorption/desorption. Based on this criterion, the sites on top of O of oxide δ-(111)-Mo, on top of C of hydroxyl G-(110), and hcp site of oxide η-(001)-Mo are regarded to be catalytically favorable. The values of ΔG_H were further optimized by considerations of different hydrogen coverages. Based on the hydrogen coverage determined by hydrogen adsorption ability on each surface, the calculated exchange current densities for every potential facet were combined into a volcano plot (Figure 6b). Nine surfaces were found to exhibit an exchange current density larger than 0.1 mA/cm^2. It is interesting that most of them are terminated with carbon atoms and not covered by either oxygen or hydroxyl. This result suggests positive effects from surface carbon sites and inferior adsorption of water on Mo_xC surfaces for HER.

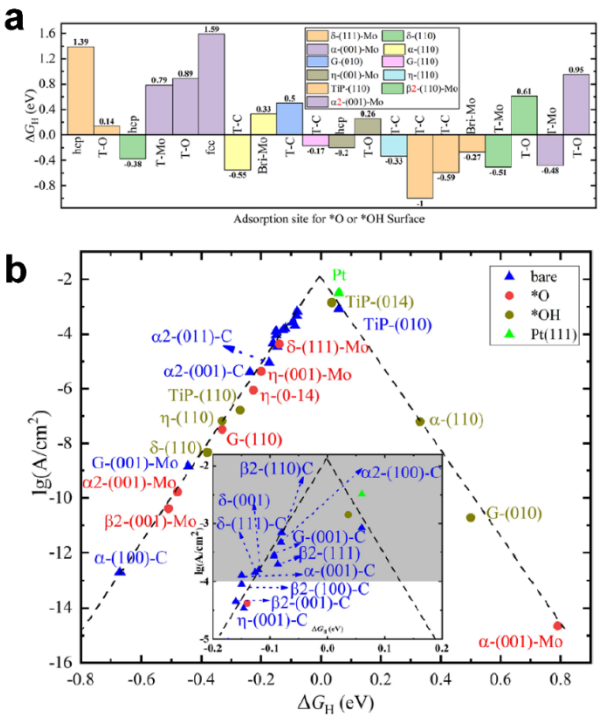

Figure 6. (**a**) Free-energy change of adsorbed H (ΔG_H) on different sites of O* and HO* surfaces. δ, α, G, η, TiP refer to different Mo_xC crystal phases and structures. (**b**) Exchange current densities as a function of hydrogen adsorbed free energy for MoC and Mo_2C surfaces. The grey area indicates the corresponding surfaces which exhibit an exchange current density larger than 0.1 mA/cm^2. α2 and β2 represents α-MoC and β-Mo_2C, respectively. Reprinted with permission from Ref. [11].

The above simulation data highlights the effect of surface composition on catalytic properties and the potential applications to different reactions catalyzed by Mo_xC such as carbon dioxide utilization, biomass upgrading conversions, and electrochemical hydrogen generation. We examined electrocatalysis of surface oxidized Mo_xC catalysts towards HER, as this reaction is well studied and could be a good model reaction to evaluate the reactive sensitivity of catalyst surface or interface structures (Figure 7a) [45]. We performed controlled oxidation of Mo_2C nanoparticles and studied the effects of different surface compositions on HER activities (Figure 7b) [23]. The partially oxidized Mo_2C electrodes were tested for HER activity by linear scanning voltammetry (LSV). The HER polarization curves overlapped with each other for Mo_2C electrocatalysts formed under oxidative potentials up to 0.4 V (Mo_2C-0.4) and 0.6 V (Mo_2C-0.65), respectively, suggesting similar HER

catalytic properties. Based on XPS data, both carbides were partially oxidized to produce Mo oxycarbide surfaces under relatively mild oxidation conditions. For further oxidized Mo_2C-*x* (*x* represents the upper limit of oxidative potentials and is equal to 0.75, 0.85, 0.975, and 1.2 V), the HER current densities decreased continuously with the increase of value *x*, indicating that a reduced HER activity due to the surface oxidation of Mo_2C catalysts (Figure 4).

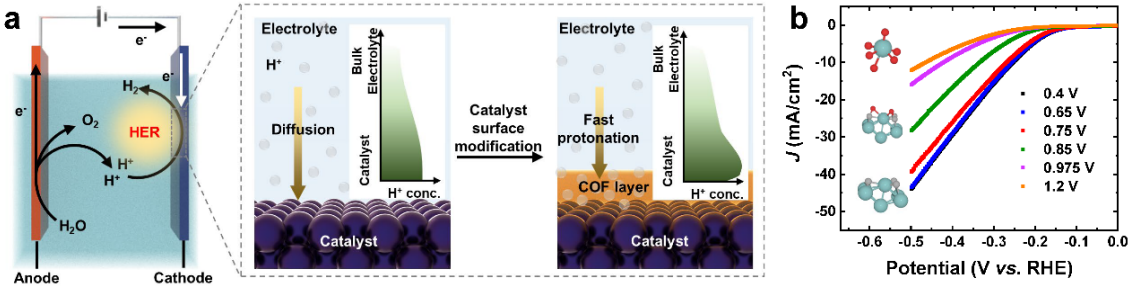

Figure 7. (**a**) Schematic illustration of electrode chemical reactions in water electrolyzer and the control of HER reactants (protons) at unmodified (**left**) and covalent organic framework-modified (**right**) electrode surfaces. Reprinted with permission from Ref. [45]. (**b**) Polarization curves of surface oxidized β-Mo_2C electrocatalysts for the HER. Insets are the corresponding illustrations of nearest neighboring atoms for a given Mo with different oxidative states formed under different upper oxidation potentials. Reprinted with permission from Ref. [23].

5. Summary

Molybdenum carbide nanomaterials are promising electrocatalysts in multiple sustainable electrochemical conversion technologies, such as hydrogen production. Unlike noble metal catalysts, metal carbides are opted to surface oxidation, especially for those highly active nm-sized particles that are favored for catalysis. Controlled surface modification could be a powerful and feasible way to affect their electrochemical applications. Precision engineering of surface compositions and structures often require a better understanding of conversion processes. We recently showed electrooxidation can be an effective method for the control of surface compositions of Mo_xC catalysts, especially those made by solid-gas phase synthesis, in which case the pristine surface with no surfactant or other capping agents can be exposed. When properly excused, different degrees of surface oxidation are readily achievable by applying predetermined oxidative potentials. In the case of nm-sized β-Mo_2C nm-sized catalysts, carbide, oxycarbide and oxide surfaces could all be controllable formed electrochemically. Quantum simulations suggest the above compositions are feasible as computational data matched well with the experimental observations. Interestingly, DFT calculation suggests imbedded carbon could also be selectively oxidized.

Experimentally, the surface oxidized β-Mo_2C electrocatalysts indeed exhibited a great deal of sensitivity to surface composition or oxidation, as being demonstrated in HER. As Mo_xC can possess different bonds with metallic, covalent, and ionic features, which result in a vastly different adsorption/desorption of reactive agents and intermediates, it is no surprise that further controlling surface composition though precision electrooxidation could be a very useful tool for post-synthesis treatment of metal carbide electrocatalysts. It is anticipated electrooxidation should be applicable to change structural parameters of transition metal carbide nanocatalysts in different phases with (or without) heteroatom dopants and varied Mo valences, opening new avenues of developing non-precious metal catalysts for scalable chemical production processes.

Author Contributions: S.Y.: Conceptualization, Writing—original draft, Writing—review & editing. H.Y.: Conceptualization, Writing—review & editing, Supervision, Resources, Funding acquisition. All authors have read and agreed to the published version of the manuscript.

Funding: This work is supported in part by the National Science Foundation (CBET-2055734) and University of Illinois Urbana-Champaign (UIUC).

Data Availability Statement: Not applicable.

Conflicts of Interest: The authors declare no conflict of interest.

References

1. Huang, L.; Zheng, X.; Gao, G.; Zhang, H.; Rong, K.; Chen, J.; Liu, Y.; Zhu, X.; Wu, W.; Wang, Y.; et al. Interfacial electron engineering of palladium and molybdenum carbide for highly efficient oxygen reduction. *J. Am. Chem. Soc.* **2021**, *143*, 6933–6941.

2. Ge, R.; Huo, J.; Sun, M.; Zhu, M.; Li, Y.; Chou, S.; Li, W. Surface and interface engineering: Molybdenum carbide–based nanomaterials for electrochemical energy conversion. *Small* **2021**, *17*, 1903380.
3. Wu, J.; Yang, H. Platinum-based oxygen reduction electrocatalysts. *Acc. Chem. Res.* **2013**, *46*, 1848–1857.
4. Yu, S.; Yang, H. Design principles for the synthesis of platinum–cobalt intermetallic nanoparticles for electrocatalytic applications. *Chem. Comm.* **2023**, *59*, 4852–4871.
5. Tong, Y.; Zhang, Z.; Hou, Y.; Yan, L.; Chen, X.; Zhang, H.; Wang, X.; Li, Y. Recent progress of molybdenum carbide based electrocatalysts for electrocatalytic hydrogen evolution reaction. *Nanoscale* **2023**, *15*, 14717–14736.
6. Zhang, X.; Shi, C.; Chen, B.; Kuhn, A.N.; Ma, D.; Yang, H. Progress in hydrogen production over transition metal carbide catalysts: challenges and opportunities. *Curr. Opin. Chem. Eng.* **2018**, *20*, 68–77.
7. Liu, S.; Lin, Z.; Wan, R.; Liu, Y.; Liu, Z.; Zhang, S.; Zhang, X.; Tang, Z.; Lu, X.; Tian, Y. Cobalt phosphide supported by two-dimensional molybdenum carbide (MXene) for the hydrogen evolution reaction, oxygen evolution reaction, and overall water splitting. *J. Mater. Chem. A* **2021**, *9*, 21259–21269.
8. Zhang, B.; Zhou, J.; Elliott, S.R.; Sun, Z. Two-dimensional molybdenum carbides: Active electrocatalysts for the nitrogen reduction reaction. *J. Mater. Chem. A* **2020**, *8*, 23947–23954.
9. Li, Z.; Attanayake, N.H.; Blackburn, J.L.; Miller, E.M. Carbon dioxide and nitrogen reduction reactions using 2D transition metal dichalcogenide (TMDC) and carbide/nitride (MXene) catalysts. *Energy Environ. Sci.* **2021**, *14*, 6242–6286.
10. Wan, J.; Liu, Q.; Wang, T.; Yuan, H.; Zhang, P.; Gu, X. Theoretical investigation of platinum-like catalysts of molybdenum carbides for hydrogen evolution reaction. *Solid State Commun.* **2018**, *284–286*, 25–30.
11. Yu, G.-Q.; Huang, B.-Y.; Chen, X.; Wang, D.; Zheng, F.; Li, X.-B. Uncovering the surface and phase effect of molybdenum carbides on hydrogen evolution: A first-principles study. *J. Phys. Chem. C* **2019**, *123*, 21878–21887.
12. Wang, W.; Geng, W.; Zhang, L.; Zhao, Z.; Zhang, Z.; Ma, T.; Cheng, C.; Liu, X.; Zhang, Y.; Li, S. Molybdenum oxycarbide supported Rh-clusters with modulated interstitial C–O microenvironments for promoting hydrogen evolution. *Small* **2023**, *19*, 2206808.
13. Deng, B.; Wang, Z.; Chen, W.; Li, J.T.; Luong, D.X.; Carter, R.A.; Gao, G.; Yakobson, B.I.; Zhao, Y.; Tour, J.M. Phase controlled synthesis of transition metal carbide nanocrystals by ultrafast flash Joule heating. *Nat. Comm.* **2022**, *13*, 262.
14. Shrestha, A.; Gao, X.; Hicks, J.C.; Paolucci, C. Nanoparticle size effects on phase stability for molybdenum and tungsten carbides. *Chem. Mater.* **2021**, *33*, 4606–4620.
15. Hu, Z.; Zhang, L.; Huang, J.; Feng, Z.; Xiong, Q.; Ye, Z.; Chen, Z.; Li, X.; Yu, Z. Self-supported nickel-doped molybdenum carbide nanoflower clusters on carbon fiber paper for an efficient hydrogen evolution reaction. *Nanoscale* **2021**, *13*, 8264–8274.
16. Kuhn, A.N.; Park, R.C.; Yu, S.; Gao, D.; Zhang, C.; Zhang, Y.; Yang, H. Valorization of carbon dioxide into C1 product via reverse water gas shift reaction using oxide-supported molybdenum carbides. *Carbon Future* **2024**, *1*, 9200011.
17. Li, J.-S.; Wang, Y.; Liu, C.-H.; Li, S.-L.; Wang, Y.-G.; Dong, L.-Z.; Dai, Z.-H.; Li, Y.-F.; Lan, Y.-Q. Coupled molybdenum carbide and reduced graphene oxide electrocatalysts for efficient hydrogen evolution. *Nat. Commun.* **2016**, *7*, 11204.
18. Zhao, T.; Lan, D.; Jia, Z.; Gao, Z.; Wu, G. Hierarchical porous molybdenum carbide synergic morphological engineering towards broad multi-band tunable microwave absorption. *Nano Res.* **2024**, *17*, 9845–9856.
19. Baek, D.S.; Lee, J.; Kim, J.; Joo, S.H. Metastable phase-controlled synthesis of mesoporous molybdenum carbides for efficient alkaline hydrogen evolution. *ACS Catal.* **2022**, *12*, 7415–7426.
20. Wang, H.; Diao, Y.; Gao, Z.; Smith, K.J.; Guo, X.; Ma, D.; Shi, C. H_2 production from methane reforming over molybdenum carbide catalysts: From surface properties and reaction mechanism to catalyst development. *ACS Catal.* **2022**, *12*, 15501–15528.
21. Upadhyay, S.; Pandey, O.P. Synthesis and electrochemical applications of molybdenum carbide: Recent progress and perspectives. *J. Electrochem. Soc.* **2022**, *169*, 016511.
22. Guardia-Valenzuela, J.; Bertarelli, A.; Carra, F.; Mariani, N.; Bizzaro, S.; Arenal, R. Development and properties of high thermal conductivity molybdenum carbide–graphite composites. *Carbon* **2018**, *135*, 72–84.
23. Yu, S.; Gautam, A.K.; Gao, D.; Kuhn, A.N.; He, H.; Mironenko, A.V.; Yang, H. Implication of surface oxidation of nanoscale molybdenum carbide on electrocatalytic activity. *J. Mater. Chem. A* **2024**, *12*, 15163–15176.
24. Yang, Q.; Sun, K.; Xu, Y.; Ding, Z.; Hou, R. Tuning crystal phase of molybdenum carbide catalyst to induce the different selective hydrogenation performance. *Appl. Catal. A* **2022**, *630*, 118455.
25. Xiao, T.-c.; York, A.P.E.; Williams, V.C.; Al-Megren, H.; Hanif, A.; Zhou, X.-y.; Green, M.L.H. Preparation of molybdenum carbides using butane and their catalytic performance. *Chem. Mater.* **2000**, *12*, 3896–3905.
26. Tacey, S.A.; Jankousky, M.; Farberow, C.A. Assessing the role of surface carbon on the surface stability and reactivity of β-Mo_2C catalysts. *Appl. Surf. Sci.* **2022**, *593*, 153415.
27. Wyvratt, B.M.; Gaudet, J.R.; Thompson, L.T. Effects of passivation on synthesis, structure and composition of molybdenum carbide supported platinum water–gas shift catalysts. *J. Catal.* **2015**, *330*, 280–287.
28. Likith, S.R.J.; Farberow, C.A.; Manna, S.; Abdulslam, A.; Stevanović, V.; Ruddy, D.A.; Schaidle, J.A.; Robichaud, D.J.; Ciobanu, C.V. Thermodynamic stability of molybdenum oxycarbides formed from orthorhombic Mo_2C in oxygen-rich environments. *J. Phys. Chem. C* **2018**, *122*, 1223–1233.

29. Yu, W.; Salciccioli, M.; Xiong, K.; Barteau, M.A.; Vlachos, D.G.; Chen, J.G. Theoretical and experimental studies of C–C versus C–O bond scission of ethylene glycol reaction pathways via metal-modified molybdenum carbides. *ACS Catal.* **2014**, *4*, 1409–1418.
30. Murugappan, K.; Anderson, E.M.; Teschner, D.; Jones, T.E.; Skorupska, K.; Román-Leshkov, Y. Operando NAP-XPS unveils differences in MoO_3 and Mo_2C during hydrodeoxygenation. *Nat. Catal.* **2018**, *1*, 960–967.
31. Kumar, A.; Bhan, A. Oxygen content as a variable to control product selectivity in hydrodeoxygenation reactions on molybdenum carbide catalysts. *Chem. Eng. Sci.* **2019**, *197*, 371–378.
32. Ammal, S.C.; Heyden, A. Active site identification for glycerol hydrodeoxygenation over the oxygen modified molybdenum carbide surface. *ACS Catal.* **2023**, *13*, 7499–7513.
33. Politi, J.R. d. S.; Viñes, F.; Rodriguez, J.A.; Illas, F. Atomic and electronic structure of molybdenum carbide phases: bulk and low Miller-index surfaces. *Phys. Chem. Chem. Phys.* **2013**, *15*, 12617–12625.
34. Ma, Y.; Guan, G.; Hao, X.; Cao, J.; Abudula, A. Molybdenum carbide as alternative catalyst for hydrogen production–A review. *Renewable Sustainable Energy Rev.* **2017**, *75*, 1101–1129.
35. Liu, X.; Salahub, D.R. Application of topological analysis of the electron localization function to the complexes of molybdenum carbide nanoparticles with unsaturated hydrocarbons. *Can. J. Chem.* **2016**, *94*, 282–292.
36. Ren, J.; Huo, C.-F.; Wang, J.; Cao, Z.; Li, Y.-W.; Jiao, H. Density functional theory study into the adsorption of CO_2, H and CH_x (x = 0–3) as well as C_2H_4 on α-Mo_2C(0001). *Surf. Sci.* **2006**, *600*, 2329–2337.
37. Zhao, L.; Yuan, H.; Sun, D.; Jia, J.; Yu, J.; Zhang, X.; Liu, X.; Liu, H.; Zhou, W. Active facet regulation of highly aligned molybdenum carbide porous octahedrons via crystal engineering for hydrogen evolution reaction. *Nano Energy* **2020**, *77*, 105056.
38. Wu, N.; Liu, J.; Zhao, W.; Du, J.; Zhong, W. Molybdenum carbide MXene embedded with nickel sulfide clusters as an efficient electrocatalyst for hydrogen evolution reaction. *Int. J. Hydrogen Energy* **2023**, *48*, 17526–17535.
39. Yang, C.; Zhao, R.; Xiang, H.; Wu, J.; Zhong, W.; Li, X.; Zhang, Q. Structural transformation of molybdenum carbide with extensive active centers for superior hydrogen evolution. *Nano Energy* **2022**, *98*, 107232.
40. Sullivan, M.M.; Bhan, A. Acid site densities and reactivity of oxygen-modified transition metal carbide catalysts. *J. Catal.* **2016**, *344*, 53–58.
41. Yao, S.; Yan, B.; Jiang, Z.; Liu, Z.; Wu, Q.; Lee, J.H.; Chen, J.G. Combining CO_2 reduction with ethane oxidative dehydrogenation by oxygen-modification of molybdenum carbide. *ACS Catal.* **2018**, *8*, 5374–5381.
42. Sullivan, M.M.; Held, J.T.; Bhan, A. Structure and site evolution of molybdenum carbide catalysts upon exposure to oxygen. *J. Catal.* **2015**, *326*, 82–91.
43. Sullivan, M.M.; Bhan, A. Effects of oxygen coverage on rates and selectivity of propane-CO_2 reactions on molybdenum carbide. *J. Catal.* **2018**, *357*, 195–205.
44. Gautam, A.K.; Yu, S.; He, H.; Yang, H.; Mironenko, A.V. Role of surface oxygen in α-MoC catalyst stability and activity under electrooxidation conditions. *ChemRxiv* **2024**. https://doi.org/10.26434/chemrxiv-2024-xwh17.
45. Park, J.H.; Lee, C.H.; Yu, S.; Kharel, P.; Choi, R.; Zhang, C.; Huang, P.Y.; Kwon, J.S.-I.; Yang, H. Effects of amine-based covalent organic framework on platinum electrocatalyst performance towards hydrogen evolution reaction. *Nano Energy* **2024**, *128*, 109947.